RSC Advances

ROYAL SOCIETY OF CHEMISTRY

www.rsc.org/advances

Effects of iron or manganese doping in ZnO nanoparticles on their dissolution, ROS generation and cytotoxicity

Hong Yin*, Philip S. Casey

[*] Hong Yin. Corresponding-Author, Philip S. Casey
CSIRO Materials Science and Engineering
Clayton VIC 3168, Australia
E-mail: Hong.Yin@csiro.au

Abstract

ZnO nanoparticles (NPs) have found wide applications due to their unique optoelectronic and photocatalytic characteristics. However, their safety aspect remains a concern especially considering that they are common constituents in sunscreen formulation. Production of reactive oxygen species (ROS) and dissolution of particle to ionic zinc are identified as two key determinants for the toxicity paradigm of ZnO. Doping transitional metal into ZnO lattice has been demonstrated effective in suppressing NP dissolution and lowering cytotoxicity. However, the possibility of triggering excessive ROS by these transition metals has not been discussed. In this study, the behaviour of particle dissolution and ability of ROS generation of iron and manganese doped ZnO NPs were studied in details and further correlated with their cytotoxicity. Although Fe doping significantly reduced the level of released Zn ions, the cytotoxicity did not decrease as expected compared with undoped ZnO because more ROS were activated and damaged cells through oxidative stress. For Mn-doped ZnO NPs, their dramatically elevated intracellular ROS level was associated with high cytotoxicity compared with undoped ZnO even though both of them released similar amount of free Zn ions.

1. Introduction

Nano-sized zinc oxide (ZnO) particles possess unique catalytic, UV-absorbing, electronic, optoelectronic and photocatalytic properties, and are widely used as anti-microbials, anti-corrosives, UV-protective coatings (paints, varnishes), gas sensors, capacitors, conductive thin-films, and solar cells [1,2]. In addition, ZnO nanoparticles (NPs) are common constituents of personal care products including cosmetics and sunscreens because they efficiently absorb ultraviolet light and are also highly transparent to visible light, but larger submicrometer- and micrometer-sized ZnO particles do not have this combination of properties. Such widespread and expanding production and use of ZnO NPs increase the potential for their exposure on humans and release to the environment. Some recent studies showed that ZnO NPs can be toxic to a wide variety of biological systems, including epidermal cells [3], bacteria (Streptococcus agalactiae and Staphylococcus aureus) [4], zebra fish (Danio rerio) [5], and mice [6]. Moreover, ZnO was more toxic to Escherichia coli than other metal oxide NPs such as Fe_2O_3, Y_2O_3, TiO_2, and CuO [7].

The mechanisms of ZnO cytotoxicity have been intensively studied and production of reactive oxygen species (ROS) as a result of cell interaction with NPs is one of the toxicity paradigms [8,9]. ROS are highly reactive ions or very small molecules and include oxygen ions, free radicals, and peroxides. In normal conditions, ROS are generated at low levels and are neutralized by antioxidant enzymes. When the magnitude of ROS overwhelms the antioxidant cellular defence, forcing the cell to enter a state of oxidative stress, various damages were stimulated to different cellular components such as proteins, lipids and DNA [10,11]. Lipovsky et al demonstrated that ZnO NPs could produce a variety of free radicals in the presence of *C. albicans* and the cytotoxic effect was mediated by introducing a free radical scavenger (histidine) to the cultures [12]. Depending on the relative abundance of ROS and the type of cellular pathways that are engaged by oxidative stress, excessive ROS can induce cell membrane damage, which may lead to cell death [13,14] or facilitate accumulation and internalization of the NPs into cells and cause toxicity [15,16]. On the other hand, some reports agreed that substantial particle dissolution to ionic zinc was another determinant for toxicity of ZnO NPs [17,18]. Deng et al concluded from their investigation on ZnO NPs exposure to neural stem cells that toxicity resulted from dissolved Zn^{2+} in the culture medium or inside cells [19]. Recent study by Sasidharan et al demonstrated that rapid dissolution of ZnO nanocrystals in acidic cancer microenvironment led to higher cytotoxicity

towards cancer cells than primary cells [20]. In addition, pH-triggered intracellular release of ionic Zn^{2+} was found to be responsible for the toxicity of ZnO nanowires [21]. Furthermore, a correlation between free Zn ions and overall ROS generation was also proposed. Gilbert et al found that released Zn ions were capable of ROS generation and activation of an integrated cytotoxic pathway that included intracellular calcium flux, mitochondrial depolarization, and plasma membrane leakage [22]. Similarly Zhu et al reported that both ZnO NPs and released Zn ions contributed to the toxicity to zebrafish embryos by increasing ROS level and/or compromising the cellular oxidative stress response [23].

Following the understanding of possible reasons accounted for ZnO toxicity, several attempts have been made to design a potentially safer ZnO. Yin et al reported that serum-coated ZnO NPs could exhibit low cytotoxicity and genotoxicity to WIL2-NS human lymphoblastoid cells compared with uncoated NPs, which was associated with low intracellular ROS generation [24]. George et al suggested that doping iron as secondary element into the lattice of ZnO NPs could reduce the toxicity in bronchial epithelial and macrophage cell lines [25]. Subsequent studies compared the effects of undoped to Fe doped ZnO NPs in rat lung, mouse lung, and zebrafish embryo and demonstrated that Fe doped particles exhibit a reduced toxicity compared to undoped ZnO in all three animal models. Slower rate of Zn ion released from Fe-doped NPs was the main reason attributed to above reduced in vitro and in vivo toxicity [26]. However, addition of transitional metal with variable valence, such as Fe, into ZnO NPs could activate a Fenton-type reaction and increase the ability to generate more ROS. This potential issue which may compromise the low toxicity rendering by reduced dissolution through Fe doping was not discussed in details. Moreover compared with ZnO NPs doped with Fe, the effect of other transitional metal doping were scarcely reported [27]. In this article, we investigated the cytotoxicity of ZnO NPs doped with iron or manganese in comparison with that of undoped ZnO NPs. Both particle dissolution and ROS generation were measured and compared to elucidate the toxicity mechanisms of ZnO NPs.

2. Materials and methods

2.1. Materials

Precursors to prepare ZnO particles were purchased from Sigma-Aldrich. Biological reagents used for experiments with cells, such as RPMI 1640 medium, fetal bovine serum(FBS), L-glutamine (200mM), penicillin/streptomycin (with 10 000 units penicillin and 10 mg of streptomycin/mL), 2,7-dichlorofluoroscein diacetate (DCFH-DA, 97%), 3-(4,5-dimethylthiazol-2-yl)-2,5-diphenyltetrazolium bromide (methyl tetrazolium, MTT, 97.5%), phosphate-buffered saline (PBS, pH 7.4 biotechnology performance certified), and sodium dodecyl sulfate (SDS, 99.9%) were also purchased from Sigma-Aldrich. Supplemented RPMI1640 medium was prepared by mixing 92 vol % RPMI1640 medium, 5 vol % FBS, 1 vol % L-glutamine, and 1 vol% penicillin/streptomycin.

2.2 Preparation of NPs

Both doped and undoped ZnO particles were prepared using a proprietary process developed by CSIRO Materials Science and Engineering (Melbourne, Australia). Interested readers may contact the corresponding author to discuss the supply of these ZnO NPs for academic research. To fabricate Fe-doped and Mn-doped ZnO NPs, precursors containing Fe and Mn were used to achieve nominal 2 wt. % in final products. Actual doping concentration was determined after synthesis.

2.3 Physico-chemical characterizations

Actual doping concentration was quantified with inductively coupled plasma-atomic emission spectroscopy (ICP-AES, Varian Vista AX Simultaneous Axial) after digesting the NPs. Crystalline phases were identified by X-ray diffraction (XRD) using a Bruker D8 Advance diffractometer. The local atomic environment was investigated using extended X-ray absorption fine structure (EXAFS). The morphologies of the particles were studied using images taken on a Transmission Electron Microscope (TEM, JEOL, 100CX-II, Japan). The particles (~10 mg) were dispersed in 5 ml deionised water. The dispersion was subject to ultrasonication for 30 min and a droplet of the dispersion was placed on a carbon coated copper grid and allowed to dry overnight. The particle size and distribution were assessed by measuring the dimensions of about 100 particles. Surface chemistry were analysed by X-ray photoelectron spectroscopy (XPS; ESCA LAB 220i-XL Thermo VG Scientific, U.K.). XPS data files were processed using the application CasaXPS software (version 2.3.13). Zeta potentials and hydrodynamic diameters of ZnO NPs in deionised water and supplemented RPMI1640 cell culture medium were determined using a Malvern Nano Z Zetasizer. 10 mg

ZnO NPs were dispersed in a cuvette containing 3 ml deionised water or supplemented RPMI1640 cell culture medium and was put in an ultrasonic bath for 10 seconds and then shaken manually to ensure good dispersion. Zeta potential and hydrodynamic diameter of each sample were measured 5 times and an average was determined.

2.4 Cytotoxicity-MTT assay

WIL2-NS human lymphoblastoid cells were cultured and maintained in supplemented RPMI 1640 medium. Cells were seeded into 96-well plates with each well receiving a volume of 100 µl at a density of $1x10^5$ cells/mL. ZnO particles were suspended in supplemented RPMI 1640 medium at twice the desired final concentrations of 50, 35, 20, 10 mg/L and ultrasonicated for 30 min to minimize agglomeration. Then 100 µL of each particle suspension was added to the test cells, and 100 µl of supplemented medium with no ZnO particles was added to the control cells. Cells in plates were cultured at 37 ^oC under a humidified atmosphere with 5% CO_2 for 24 h. MTT was dissolved in PBS at 5 mg/mL, and then 20 µL of this solution was added to each well to give a concentration of 0.5 mg/mL. The cells were incubated at 37 ^oC for another 3 h, after which 80 µL of 20% SDS in 0.02M HCl was added to each well and mixed thoroughly, and the cells were incubated for another 4 h. The optical density (OD) at 570 nm was determined using an ELISA microplate reader (MPR-30-6VP) with 630 nm as a reference wavelength. The OD of the background was determined using supplemented medium containing particles but no cells. The results are presented as the percentage viability of cells exposed to ZnO NPs relative to cells not exposed.

2.5 Dissolution of ZnO particles

Dissolution behaviour of ZnO NPs is strongly dependent on the nature of dispersion medium [28]. Relatively subtle changes in characteristics of the medium, such as pH, ionic strength, type of ions, and type of proteins present in the medium, can greatly alter interfacial morphology, hydrophobicity, and charge, which consequently lead to variations in solubility [29]. To study whether dissolution is a key factor influencing cytotoxicity, solubility of ZnO NPs was measured in the supplemented cell culture medium without the presence of cells. ZnO NPs (5 mg) were put into 50 mL of supplemented RPMI 1640 cell culture medium in a plastic tube and the resulting ZnO concentration was 100 mg/L. The plastic tube was placed in a water bath shaker maintained at 37^oC. At each time interval (0 h, 2 h, 6 h, 24 h, 48 h and 120 h), 1.5 mL aliquots were taken out from the suspension and centrifuged at 10,000 rpm for

30 min; 1 mL of supernatant was added to 9 mL of supplemented RPMI 1640 cell culture medium, and the resulting zinc solution was digested and followed by elemental analysis to determine Zn concentration. Mn and Fe concentration in the same aliquot was also measured by ICP-AES.

2.6 ROS generation

Levels of ROS generated by ZnO particles in the presence of cells were determined by a fluorometric assay using the intracellular oxidation of DCFH-DA. Cells grown to confluence 24 h after seeding were treated with particles at a concentration of 10 mg/L or 20mg/L for 24 h, washed with PBS, and then incubated with 40 μM DCFH-DA for 30 min. At the end of the incubation, cells were washed with PBS again. The fluorescence of dichlorofluoroscein (DCF), which is the oxidized product of dichlorofluoroscein (DCFH, hydrolyzed from DCFH-DA by intracellular esterases), was measured with a Perkin Elmer Victor 3 1420 multilabel plate counter using an excitation of 485 nm and an emission of 530 nm. The DCF concentration in WIL2-NS cells not exposed to ZnO particles was used as a control.

3. Results and discussions

3.1 Characterisation

The actual doping concentration in ZnO NPs was identified as 2.1 wt% for Fe and 0.8 wt% for Mn. Because precursors containing Fe or Mn were used in the synthesis to achieve nominal 2 wt% in both ZnO NPs, our results indicate that Mn is more difficult to be incorporated into ZnO lattice. This finding is in line with earlier reports, showing a larger divergence in ionic sizes between Mn^{2+} (0.83Å) and Zn^{2+} (0.74 Å) could be attributed to a lower Mn concentration in Mn-doped ZnO [30,31]. Comparatively, Fe^{2+} with an ionic diameter 0.77Å that is comparable to the size of Zn^{2+}, allows an easy substitution.

X-ray diffraction patterns shown in Figure 1a suggest that the internal structure (long range order) is the same for doped and undoped NPs with hexagonal wurtzite ZnO being the only phase identified. No additional peaks from secondary phase were observed for doped ZnO, corroborating that Mn or Fe acts as a substitutional dopant. The local atomic environment was investigated using EXAFS and Figures 1b shows the spectra of Fourier-transform amplitude versus radial distance of Zn K-edge. Two strong peaks were identified in all three

types of ZnO NPs at approximately 1.5Å and 2.9 Å corresponding to Zn-O and Zn-Zn shells respectively. Compared with undoped ZnO, doped ZnO have similar Zn-O shell intensity (R=1.5Å), whereas the intensity at R=2.9 Å (Zn-Zn shell) was significantly lower. It implies that some Zn atoms had been replaced by dopant in the short range order. The spectra of Mn-doped ZnO and Fe-doped ZnO are generally similar, except that the latter has higher Fourier-transform amplitude in Zn-Zn shell, agrees well with the higher Fe concentration detected in Fe-doped ZnO NPs. The schematic diagrams shown in Figure 1c illustrate the structures of undoped and doped ZnO NPs indicating that hexagonal wurtzite of ZnO did not change after doping. Doping atoms (Fe or Mn) may disturb the local environment of Zn leading to lower Fourier-transform amplitude in Zn-Zn shell (R=2.9 Å).

The morphology of doped and undoped ZnO NPs was studied using TEM and the typical images are shown in Figure 2. It is noticed that shape of particles, size distribution and state of agglomeration are largely similar between doped and undoped ZnO. However, undoped ZnO NPs have larger particle size than doped ones. Quantitatively, the primary particle sizes determined by averaging the diameters of 100 particles are 25.8±8.9 nm, 12.2±2.7 nm and 16.5±5.9 nm for undoped, Fe-doped and Mn-doped ZnO NPs respectively. As reported by Sahu et al, shrinkage of particle size in doped NPs could be related to inhibition of the grain growth when doping atoms were present [32]. Because of the higher doping concentration (2.1 wt. %), it is not surprising to find that Fe doped ZnO has the smallest particle size.

Particle surface was analysed by XPS and the survey spectra shown in Figure 3a did not reveal any evident differences between doped and undoped ZnO NPs. Refined scans focusing on Fe 2p (Figure 3b) and Mn 2p (Figure 3c) core levels were able to resolve Fe 2p 1/2 (722.3eV), Fe 2p 3/2 (708.5eV) and Mn 2p 3/2 (638.8eV) from some major peaks originated to Zn Auger emissions. Figure 3(d) shows the high resolution spectra of Mn 3p core level which is a spectral region free from on any interference, confirming the presence of Fe or Mn in the doped ZnO NPs. To study surface charge in aqueous medium, zeta potentials measured in deionised water (pH=6.0) and supplemented RPMI1640 medium (pH=7.4) are shown in Table 1. Undoped, Fe-doped and Mn-doped ZnO NPs exhibited zeta potentials of 16.1 mV, 12.2 mV and 10.6 mV respectively in water, consistent with the reported isoelectric point of ZnO being between 8 and 9 [33]. When zeta potentials were measured in supplemented RPMI1640 medium, all three types of ZnOs exhibited negative charges (-7.5mV~-10mV) due to surface adsorption of proteins from medium [34]. Hydrodynamic diameters of ZnO

NPs measured by DLS in both deionised water and supplemented RPMI1640 medium are also listed in Table 1. ZnO NPs showed average hydrodynamic diameters varying from 500-700 nm in water to 700-900 nm in supplemented medium. Both of the diameters are significantly larger than the primary particle sizes determined by TEM, indicating the presence of a large amount of agglomerations.

3.2 Cytotoxicity

Cell viability was assessed by MTT assay, which measures mitochondrial reductase activity. Figure 4 shows the relationship between cell viability and the concentration of ZnO NPs for WIL2-NS cells cultured for 24 h in the presence of undoped or doped ZnO NPs. At low NP concentration (2 mg/L), all three types of ZnO had high cell viability. Slight cellular activity stimulation (mitochondrial reductase activity is higher than untreated control 100%) was observed in doped ZnO NPs (viability 112% for Fe-doped ZnO and 109% for Mn-doped ZnO), but not in undoped ZnO (viability 98%). Such beneficial response at a low dose exposure found in doped ZnO is called hormesis and has been reported in several toxicological studies involving NPs [35,36]. It is mainly triggered by hormetic mechanisms, i.e. activation of adaptive cellular stress response pathways (ACSRPs), including receptors coupled to kinases and activation of transcription factors that induce the expression of cytoprotective proteins such as antioxidant enzymes, protein chaperones, and growth factors [37].

With the increase of NP concentration, cell viability of all three types of ZnO NPs decreased. Undoped and Fe-doped NPs shared very similar viability profiles, whereas Mn-doped ZnO was much more toxic. When the NP concentration was 10mg/L, cell viabilities of undoped and Fe-doped were 92% and 102% respectively. In the same condition, only 77% cells survived after exposure to Mn-doped NPs. Cytotoxicity increased markedly at higher concentration tested (20mg/L) with cell viability 56%, 61% and 14% for undoped, Fe-doped and Mn-doped NPs respectively. When the NP concentration further increased to 35 mg/L and 50 mg/L, very low cell viabilities (less than 10%) were found in all three types of ZnO NPs. EC50 (the effective concentration corresponding to 50% cell viability) was used to compare cytotoxicity quantitatively. From Figure 4, EC50 was determined as ~22mg/L for undoped and Fe-doped NPs and ~14 mg/L for Mn-doped ones. It confirmed that the cytotoxicity ranked in the order of Mn-doped>Fe-doped≈undoped.

ICP-AES study on the aliquot after dissolution did not detect any Mn or Fe, suggesting the release of Mn or Fe from ZnO NPs is negligible. Figure 5 presents the dissolution kinetics (release of ionic Zn from ZnO NPs) in supplemented RPMI1640 cell culture medium. Equilibrium solubility of undoped ZnO was 1.8 mg/L and it was achieved within 2 hours. Comparatively, it took 120 hours for Mn-doped ZnO to reach the same equilibrium solubility, indicating that Mn doping reduced the dissolution rate. Fe-doped ZnO showed an even slower dissolution rate accompanying with a lower solubility at the maximum measuring period (120 hours). Within the cell culture duration (24 hours), significant difference was found in the amount of Zn ions released from NPs to the cell culture medium, i.e. Fe-doped ZnO released 0.8 mg/L Zn ions which is only half of Zn ions shedding from undoped ZnO (1.8 mg/L) and Mn doped ZnO (1.6 mg/L).

Dissolution of Fe-doped ZnO in various water-based dispersion media has been studied in comparison with that of undoped ZnO NPs. Xia et al reported that Fe doping (1-10 wt %) moderated Zn^{2+} dissolution in Phosphate Buffered Saline (PBS) in the presence of dipalmitoylphosphatidylcholine (DPPC) and bovine serum albumin (BSA). Fe doping of 4 wt % could restore the Zn ion concentration in the supernatant to background levels (i. e. the original Zn concentration in supplemented PBS without adding any NPs) [38]. Similarly, George et al observed a decreased rate of dissolution and a lower solubility in Fe-doped ZnO NPs compared with those of pure ZnO NPs in 0.1M sodium perchlorate solution at pH=7 [25] . In addition, reduced solubility of Fe-doped ZnO was reported by Fairbairn et al in seawater [39]. Our results demonstrating that Fe doping could suppress ZnO dissolution in supplementary RPMI1640 cell culture medium agree well with above observations. The effect of Fe doping on ZnO dissolution in these water-based dispersion media could be related to an enhanced aqueous stability of Fe-doped ZnO. Substituting Zn for Fe in ZnO matrix was proposed to strengthen the binding to oxygen and thus restrain proton-assisted dissolution [40,41].

The influence of doping on the ability of ZnO NPs to produce ROS was investigated using a fluorescence assay that specifically detects hydroxyl radicals [42]. In this assay, hydrophobic DCFH-DA molecules, which readily penetrate cellular membranes, are hydrolyzed by intracellular esterases to yield dichlorofluoroscein (DCFH), a nonfluorescent compound; DCFH can then be oxidized by hydroxyl radicals to the fluorescent compound dichlorofluorescein, DCF. Figure 6 shows relative DCF intensities produced by doped or

undoped ZnO NPs (compared with the DCF concentration in WIL2-NS cells not exposed to ZnO particles, 100%) when the NP concentration was 10 mg/L and 20 mg/L respectively.

All tested DCF intensity was higher than 100%, indicating that ROS level in the presence of ZnO particles was higher than the level without the presence of ZnO. Moreover, the ROS generation also increased with particle concentration for all three types of ZnO NPs. For both concentrations (10mg/L and 20 mg/L), increasing levels of ROS were produced in the order of undoped<Fe-doped << Mn-doped ZnO. In details, ROS level triggered by undoped ZnO NPs was slightly higher than the control, and Fe-doped ZnO produced higher ROS (120% and 132% for 10 mg/Land 20 mg/L respectively). There is a distinct increase of ROS level when cells were exposed to Mn-doped ZnO NPs in which 313% and 548% of DCF intensities were detected in comparison with control cells (100%).

Pure ZnO NPs are generally not regarded as ROS catalyst because Zn only exists in one oxidation state and cannot contribute to electron reduction in biological systems. However, ZnO can indirectly cause oxidative injure by fully occupying oxidative stress defence compounds, such as metallothionein [43]. Our observation that ROS level stimulated by undoped ZnO NPs is only slightly higher than the control also confirms that oxidative stress may not be the main consideration of ZnO toxicity. Compared with pure ZnO NPs, additional oxidative stress might be triggered in doped ZnO NPs by transitional metal ions released from particles or by catalytically active properties of NP surface. Dissolution of ZnO NPs in cell culture medium could release metal ions which were further internalisation by cells. However, cell membranes offer an excellent barrier for most of ions and restrain such cation transportation. Cellular uptake of NPs therefore has been perceived as the major transportation pathway between cells and ZnO [44]. Gilbert et al demonstrated that ZnO NP toxicity is based on nanoparticle uptake followed by intracellular dissolution [22]. For doped ZnO NPs, Fe or Mn ions could release intracellularly via dissolution and such ions with variable valence has been demonstrated to enhance the particle's ability to generate ROS by catalyzing the dissociation of H_2O_2 to a hydroxyl radical and hydroxide ion [45,46,47], or to a hydrogen ion and hydroperoxy radical [48,49] . In support of this, studies have shown that Fe^{3+} supported on bulk ZnO improved catalytic activity for H_2O_2 production [50], and introduction of free transition metal ions induced protein oxidation and redox state within cells [51]. Furthermore, ROS generation could also be reinforced on the catalytically active

surface of doped NPs. The following oxygen reduction reactions could occur with the presence of NP catalyst, leading to various ROS groups, such as superoxide anion, hydrogen peroxide and hydroxyl radical [52].

$O_2 + e^- \rightarrow O_2^{\bullet-}$ (superoxide anion)
$O_2^{\bullet-} + 2H^+ + e^- \rightarrow H_2O_2$ (hydrogen peroxide)
$H_2O_2 + e^- + H^+ \rightarrow 2\ \bullet OH$ (hydroxyl radical)
$2\bullet OH + e^- + H^+ \rightarrow H_2O$

As shown in Figure 7, Mn doped ZnO generated distinctly higher level of ROS than Fe doped ones. Considering that the Fe doping concentration (2.1 wt%) was much higher than that of Mn (0.8 wt%), this non compositional correlation may indicate that, beyond composition, other unique properties of Mn are determining the ROS generation process. Consistent with our observation, abnormally high ROS level has also been documented in several Mn-containing NPs. For example, compared with untreated control, there was a significant ROS increase (> 10-fold) in neuronal phenotype cells (PC-12) when co-cultured with 25mg/L manganese oxide NPs (40 nm) [53]. Additionally, Limbach et. al. reported that addition of as few as 1.6 wt % Mn in silica NPs afforded a ROS increase of 2500% in lung epithelial cells (A549) [54]. This elementally specific ROS production of Mn was indicated as a result of coexistence of Mn atoms of different oxidation states. Transformation between Mn(II), Mn(III) and Mn(IV) would induce d–d electron exchange interactions, thus providing the necessary electron-mobile environment for the surface redox activity [55]. It may also facilitate the formation of defects (vacancies, electrons and holes), and affect the electronic distribution on the surface which also enhance the catalytic activity of the NPs [56,57].

In summary, Fe-doped ZnO suppressed NP dissolution in cell culture medium compared with undoped NPs. However, its ability to generate higher ROS compromised the positive effect caused by less dissolution and it consequently had very similar toxic profile as undoped ZnO. Mn-doped ZnO had comparable solubility with undoped ZnO, but it produced a particularly large amount of ROS, which led to its highest toxicity among all three types. Our studies suggest that both dissolved free Zn ions and particle-induced ROS are the major sources to activate cytotoxic response of WIL2-NS cells, but no direct relationship was found between them. As a result, these two aspects should be considered concurrently when aiming to design ZnO NPs with low cytotoxicity. Doping transitional metal into ZnO lattice is likely to reduce

dissolution. However, it has the potential to increase oxidative stress at the same time. To develop an effective strategy to attain safer ZnO NPs, both lower solubility and lower ROS generating ability need to be achieved.

It is also important to mention here that above cytotoxicity and ROS results were obtained in dark, in which ZnO NPs did not provoke an appreciable ROS level. When NPs are exposed to UV light, ZnO with intrinsic photocatalytic activity could stimulate more free radicals and induce additional phototoxicity. As it has been reported, both Mn and Fe doping could alter the photocatalytic activity of ZnO, i.e. the generation of free radicals will be largely concealed in doped ZnO under UV exposure [58]. The UV-induced toxicity may also be different from what we studied here in dark. Therefore photo-induced toxicity associated with photocatalytic activity of NPs needs further investigation.

4. Conclusion

Cytotoxicity and possible mechanisms resulting in cytotoxicity, such as particle dissolution and intracellular ROS generation were investigated on Fe-doped and Mn-doped ZnO NPs together with undoped ZnO NPs. Compared with undoped ZnO, Fe doping could reduce Zn ion release and Mn doping did not have significant impact on particle dissolution. Both doping increased the intracellular ROS level whereas Mn-doped ZnO NPs showed about 450% increase at NP concentration of 20 mg/L in contrast to 30% increase when Fe-doped particles were present. The observed cytotoxicity is a combined effect of Zn ion release and intracellular ROS generation and the overall effect on cytotoxicity was that Fe doped NPs had similar toxicity as undoped NPs and Mn doped NPs were more toxic. Our results suggest that both low solubility and low ROS generating ability need to be achieved for developing an effective strategy to attain safer ZnO NPs.

Acknowledgement

This work was funded by the CSIRO Materials Science and Engineering, the CSIRO Advanced Materials Transformational Capabilities Platform, and the CSIRO Future Manufacturing Flagship. The authors thank Professor Ian Harper and Dr. Judy Callaghan (Monash University) and Ms. Carolyn Salisbury (CSIRO) for their assistance with cell

culture activities. We thank Dr. Jamie Booth, Dr. Zongli Xie, Ms. Liz Goodall, Ms. Lynne Waddington, Ms. Yeşim Gözükara**,** and Dr. Thomas Gengenbach**,** all from CSIRO, for their characterisation work using EXAFS, BET, XRD, TEM, ICP-AES, and XPS, respectively. We also wish to express our appreciation to Dr Maxine McCall (CSIRO) for her useful suggestions during manuscript preparation.

References

[1] S. L. Ji and C. H. Ye, *J. Mater. Sci. Technol.*, 2008, **24,** 457-472.
[2] Z. L. S. Seow, A. S. W. Wong, V. Thavasi, R. Jose, S. Ramakrishna and G. W. Ho, *Nanotechnology*, 2009, **20,** 045604.
[3] V. Sharma, R. K. Shukla, N. Saxena, D. Parmar, M. Das and A. Dhawan, *Toxicol. Lett.*, 2009, **185,** 211-218.
[4] Z. B. Huang, X. Zheng, D. H. Yan, G. F. Yin, X. M. Liao, Y. Q. Kang, Y. D. Yao, D. Huang and B. Q. Hao, *Langmuir*, 2008, **24,** 4140-4144.
[5] X. S. Zhu, L. Zhu, Z. H. Duan, R. Q. Qi, Y. Li and Y. P. Lang, *J. Environ. Sci. Health Part A: Environ. Sci. Eng.*, 2008, **43,** 278-284.
[6] B. Wang, W. Y. Feng, M. Wang, T. C. Wang, Y. Q. Gu, M. T. Zhu, H. Ouyang, J. W. Shi, F. Zhang, Y. L. Zhao, Z. F. Zhai, H. F. Wang and J. Wang, *J. Nanopart. Res.*, 2008, **10,** 263-276.
[7] X. K. Hu, S. Cook, P. Wang and H. M. Hwang, *Sci. Total Environ.*, 2009, **407,** 3070-3072.
[8] M. I. Setyawati, C. Y. Tay and D. T. Leong, *Biomaterials*, 2013, **34,** 10133-10142.
[9] X. S. Zhao, S. T. Wang, Y. Wu , H. You and L. N. Lv, *Aquat. Toxicol.*, 2013, **136,** 49-59.
[10] C. Hanley, J. Layne, A. Punnoose, K. M. Reddy, I. Coombs, A. Coombs, K. Feris and D. Wingett, *Nanotechnology*, 2008, **19,** 295103.
[11] H, Yang, C. Liu, D. Yang, H. Zhang and Z. Xia, *J. Appl. Toxicol.*, 2009, **29,** 69-78.
[12] A. Lipovsky, N. Yeshayahu, A. Gedanken and R. Lubart, *Nanotechnology*, 2011, **22,** 105101.
[13] L. Zhang, Y. Jiang, Y. Ding, M. Povey and D. York, *J. Nanopart. Res.*, 2007, **9,** 479-489.
[14] R. Wahab, A. Mishra, S. I. Yun, Y. S. Kim, and H. S. Shin, *Appl. Microbiol. Biotechnol.*, 2010, **87,** 1917-1925.
[15] R. Brayner, R. Ferrari-Iliou, N. Brivois, S. Djediat, M. F. Benedetti and F. Fievet, *Nano Lett.*, 2006, **6,** 866-870.
[16] Y. Xie, Y. He, P. L. Irwin, T. Jin and X. Shi, *Appl. Environ. Microbiol.*, 2011, **77,** 2325-2331.
[17] S. Lopes, F. Ribeiro, J. Wojnarowicz, W. Lojkowski, K. Jurkschat, A. Crossley, A. M. V. M. Soares and S. Loureiro*, Environ. Toxicol. Chem.*, 2014, **33,** 190-198.
[18] S. K. Misra, A. Dybowska, D. Berhanu, S. N. Luoma and E. Valsami-Jones, *Sci. Total Environ.*, 2012, **438,** 225-232.
[19] X. Y. Deng, Q. X. Luan, W. T. Chen, Y. L. Wang, M. H. Wu, H. J. Zhang and Z. Jiao, *Nanotechnology*, 2009, **20,** 115101.

[20] A. Sasidharan, P. Chandran, D. Menon, S. Raman, S. Nair and M. Koyakutty, *Nanoscale*, 2011, **3,** 3657-3669.
[21] K. H. Müller, J. Kulkarni, M. Motskin, A. Goode, P. Winship, J. N. Skepper, M. P. Ryan and A. E. Porter, *ACS Nano*, 2010, **4 ,** 6767-6779.
[22] B. Gilbert, S. C. Fakra, T. Xia, S. Pokhrel, L. Madler and A. E. Nel, *ACS Nano*, 2012, **6,** 4921-4930.
[23] X. S. Zhu, J. X. Wang, X. Z. Zhang , Y. Chang and Y. S. Chen, *Nanotechnology*, 2009, **20,** 195103.
[24] H. Yin, P. S. Casey, M. J. McCall and M. Fenech, *Langmuir*, 2010, **26,** 15399-15408.
[25] S. George, S. Pokhrel, T. Xia , B. Gilbert, Z. X. Ji, M. Schowalter, A. Rosenauer, R. Damoiseaux, K. A. Bradley, L. Madler and A. E. Nel, *ACS Nano*, 2010, **4,** 15-29.
[26] S. Pokhrel, A. E. Nel and L. Madler, *Accounts Chem. Res.,* 2013, **46,** 632-641.
[27] K. Rekha, M. Nirmala, M. G. Nair and A. Anukaliani, *Physica B*, 2010, **405,** 3180-3185.
[28] S. K. Misra, A. Dybowska, D. Berhanu, S. N. Luoma, E. Valsamj-Jones, *Sci. Total. Environ.*, 2012, **438**, 225-232.
[29] M. Li, D. H. Lin and L. Z. Zhu, *Environ. Pollut.*, 2013, **173,** 97-102.
[30] X. Y. Zhou, S. H. Ge, D. S. Yao , Y. L. Zuo and Y. H. Xiao, *Physica B*, 2008, **403,** 3336-3339.
[31] U. Ilyas, R. S. Rawat, Y. Wang, T. L. Tan, P. Lee, R. Chen, H. D. Sun, F. J. Li and S. Zhang, *Appl. Surf. Sci*., 2012, **258,** 6373-6378.
[32] M. Sahu and P. Biswas, *Nanoscale Res. Lett.*, 2011, **6,** 1-14.
[33] S.R. Kanel, S. R. Al-Abed, *J. Nanopart. Res.*, 2011, **13**, 4035-4047.
[34] E. Izak-Nau, M. Voetz, S. Eiden, A. Duschi, V. F. Puntes, *Part. Fibre. Toxicol.*, 2013, **10**, 56.
[35] I. Iavicoli , E. J. Calabrese and M. A. Nascarella, *Dose-Response*, 2010, **8,** 501-517.
[36] Z. M. Xiu , Q. B. Zhang, H. L. Puppala, V. L. Colvin and P. J. J. Alvarez, *Nano Lett.* , 2012, **12,** 4271-4275.
[37] M. P. Mattson, *Hum. Exp. Toxicol.*, 2008, **27**, 155-162.
[38] T. Xia, Y. Zhao, T. Sager, S. George, S. Pokhrel, N. Li, D. Schoenfeld, H. A. Meng, S. J. Lin, X. Wang, M. Y. Wang, Z. X. Ji, J. I. Zink, L. Madler, V. Castranova, S. Lin and A. E. Nel, *ACS Nano,* 2011, **5,** 1223-1235.
[39] E. A. Fairbairn, A. A. Keller, L. Madler, D. X. Zhou, S. Pokhrel and G. N. Cherr, *J. Hazard. Mater.*, 2011, **192,** 1565-1571.
[40] C. J. Martin, X. C. Le, T. L. Guidotti, S. Yalcin, E. Chum, R. J. Audette, C. K. Liang, B. S. Yuan, X. Zhang and J. Wu, *Am. J. Ind. Med.*, 1999, **35,** 574-580.
[41] J. P. Xiao, A. Kuc, S. Pokhrel, M. Schowalter, S. Parlapalli, A. Rosenauer, T. Frauenheim, L. Madler, L. G. M. Pettersson and T. Heine, *Small*, 2011, **7,** 2879-2886.
[42] O. Choi and Z. Q. Hu, *Environ. Sci. Technol.*, 2008, **42,** 4583-4588.
[43] C. C. Shen, S. A. James, M. D. de Jonge, T. W. Turney, P. F. A. Wright and B. N. Feltis, *Toxicol. Sci.*, 2013, **136,** 120-130.
[44] R. Bacchetta, E. Moschini, N. Santo, U. Fascio, L. Del Giacco, S. Freddi, M. Camatini and P. Mantecca, *Nanotoxicology*, 2014, **7,** 728-744.
[45] S. Lany, J. Osorio-Guillen and A. Zunger, *Phys. Rev. B*, 2007, **75,** 2412031-4.
[46] J. Hays, K. M. Reddy, N. Y. Graces, M. H. Engelhard, V. Shutthanandan, M. Luo, C. Xu, N. C. Giles, C. Wang, S. Thevuthasan and A. Punnoose, *J. Phys. Condens. Matter,* 2007, **19,** 226203-26.
[47] L. Sun, J. A. Rippon, P. G. Cookson, O. Koulaeva and X. G. Wang, *Chem. Eng. J.*, 2009, **147,** 391-398.

[48] K. Pirkanniemi and M. Sillanpaa, *Chemosphere*, 2002, **48,** 1047-1060.
[49] W. Y. Choi, A. Termin and M. R. Hoffman, *J. Phys. Chem.*, 1994, **98,** 13669-13679.
[50] I. A. Salem, *Monatshefte fur Chemie*, 2000, **131,** 1139-1150.
[51] A. Petit, F. Mwale, C. Tkaczyk, J. Antoniou, D. J. Zukor and O. L. Huk, *Biomaterials,* 2005, **26,** 4416-4422.
[52] G. D. Fang, D. M. Zhou and D. D. Dionysiou, *J. Hazard. Mater.*, 2013, **250,** 68-75.
[53] S. M. Hussain, K. Amanda, A. K. Javorina, A. M. Schrand, H. M. Duhart, S. F. Ali and J. J. Schlager, *Toxicol. Sci.*, 2006, **92,** 456-463.
[54] L. K. Limbach, P. Wick, P. Manser, R. N. Grass, A. Bruinink and W. J. Stark, *Environ. Sci. Technol.*, 2007, **41,** 4158-4163.
[55] M. A. Hasan, M. I. Zaki, L. Pasupulety and K. Kumari, *Appl. Catal. A-Gen.*, 1999, **181** 171-179.
[56] Z. R. Tian, W. Tong, J. Y. Wang, N. G. Duan, V. V. Krishnan and S. L. Suib, *Science,* 1997, **276,** 926-930.
[57]S. Guo, S. Zhang, L. Wu and S. Sun, *Angew. Chem. Int. Ed.*, 2012, **51,** 11770-11773.
[58] A. Dodd, A. McKinley, T. Tsuzuki and M. Saunders, *Mater. Chem. Phys.*, 2009, **114,** 382-386.

(a)

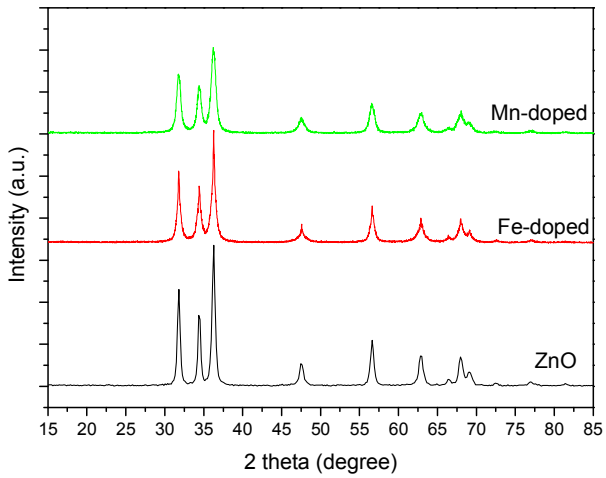

(b)

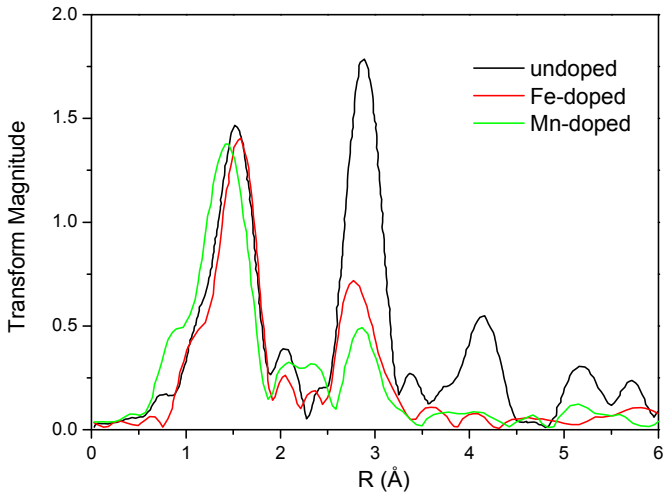

(c)

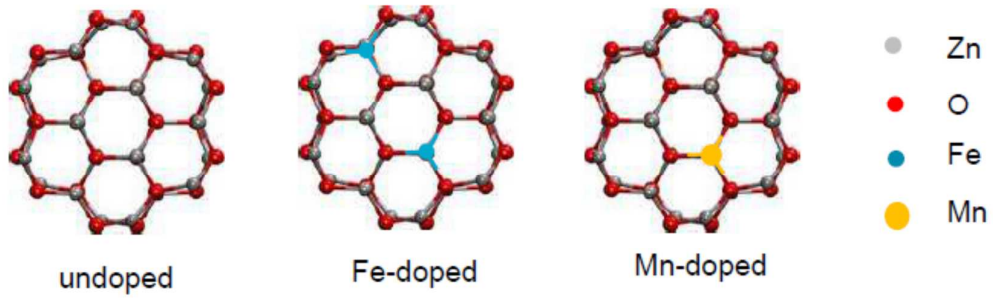

Figure 1 Long range order and short range order structural study of doped and undoped ZnO NPs. (a) x-ray diffraction patterns suggesting that the internal structure (long range order) is the same for doped and undoped NPs with hexagonal wurtzite ZnO being the only phase identified. (b) EXAFS result of Fourier-transform amplitude versus radial distance of Zn K-edge (short range order). (c) Schematic diagrams showing unchanged hexagonal structures of doped ZnO. Doping atoms disturbed local environments of Zn leading to lower Fourier-transform amplitude in Zn-Zn shell (R=2.9 Å).

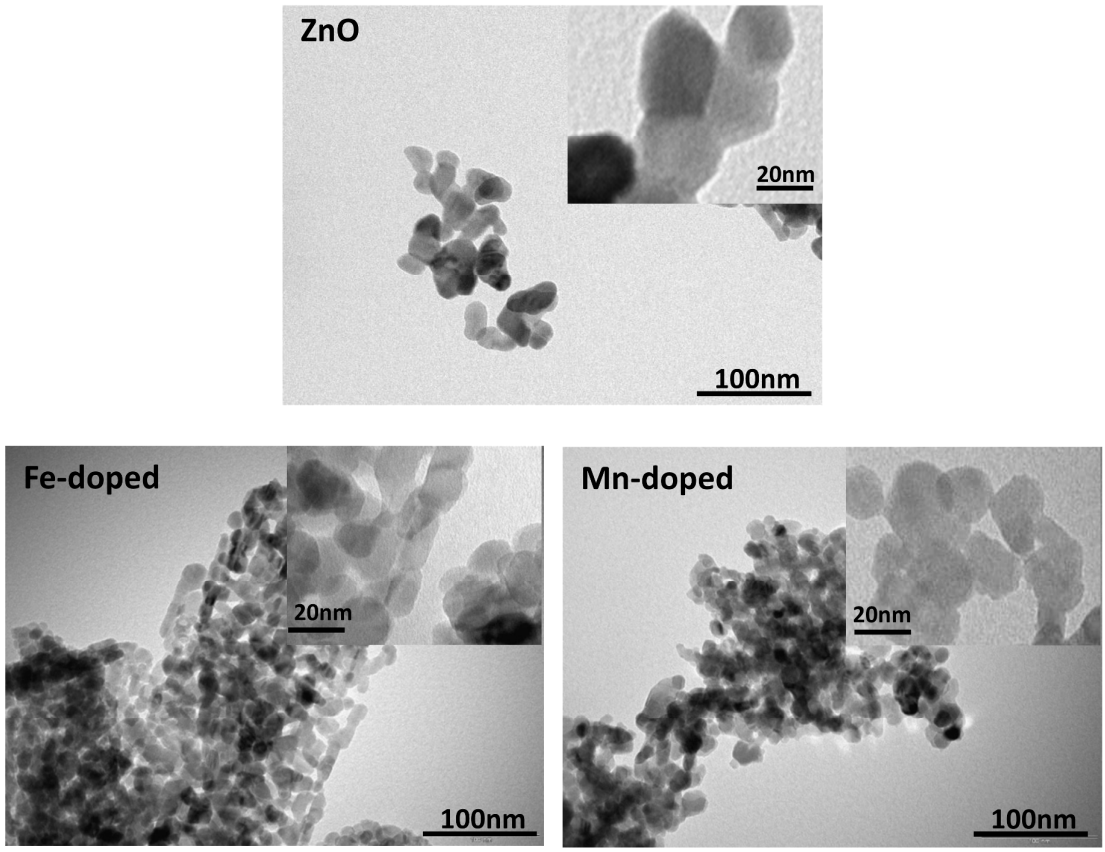

Figure 2 Typical TEM images showing morphology of three types ZnO NPs with insets showing at a higher magnification. The primary particle sizes of undoped NPs, Fe-doped ZnO and Mn-doped were 25.8±8.9 nm, 12.2±2.7 nm and16.5±5.9 nm respectively (determined by averaging the diameters of 100 particles).

(a) (b)

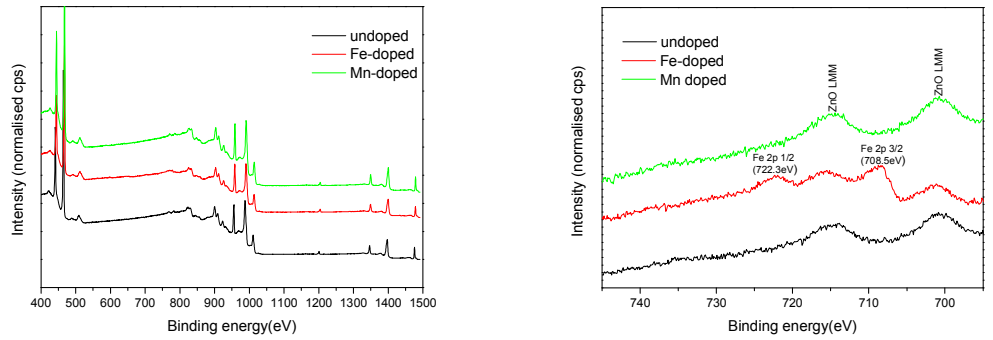

(c) (d)

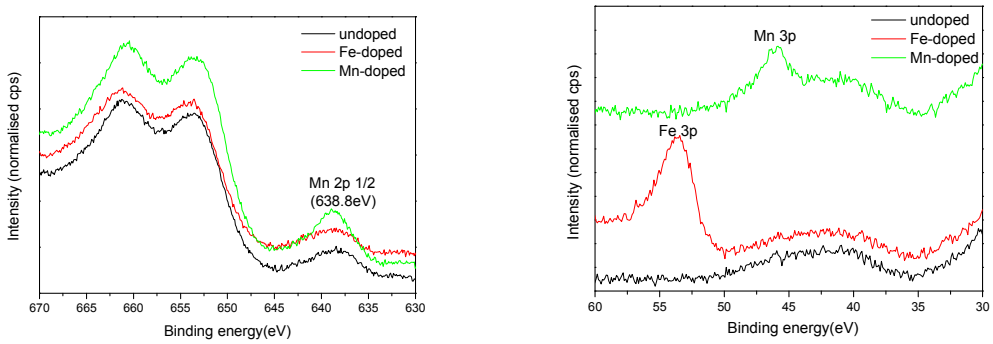

Figure 3 XPS spectra showing undoped, Fe-doped and Mn-doped ZnO NPs. (a) Survey spectra. (b) Fe 2p core level. (c) Mn 2p core level. (d) Fe/Mn 3p core level.

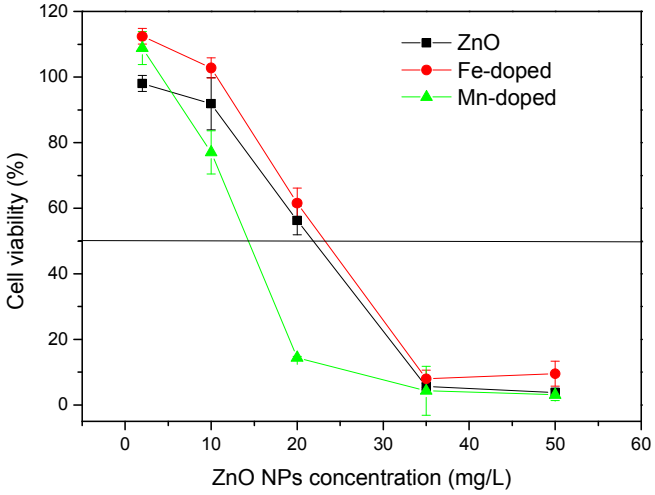

Figure 4 Relation between cell viability and the concentration of ZnO NPs for WIL2-NS cells cultured for 24 h in the presence of undoped, Fe-doped and Mn-doped ZnO NPs.

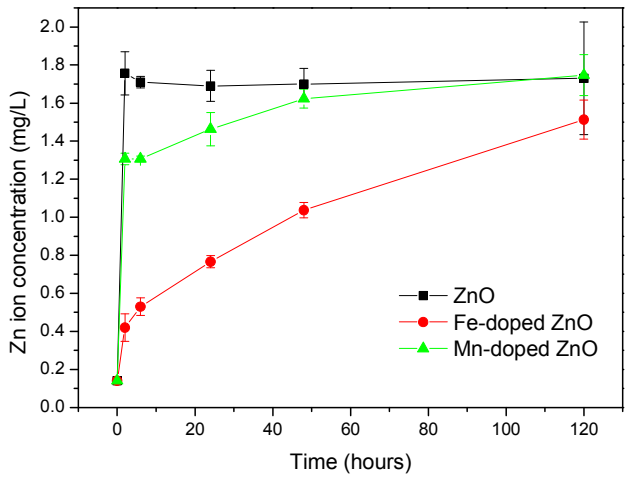

Figure 5 Dissolution kinetics of doped and undoped ZnO NPs in supplemented RPMI1640 cell culture medium.

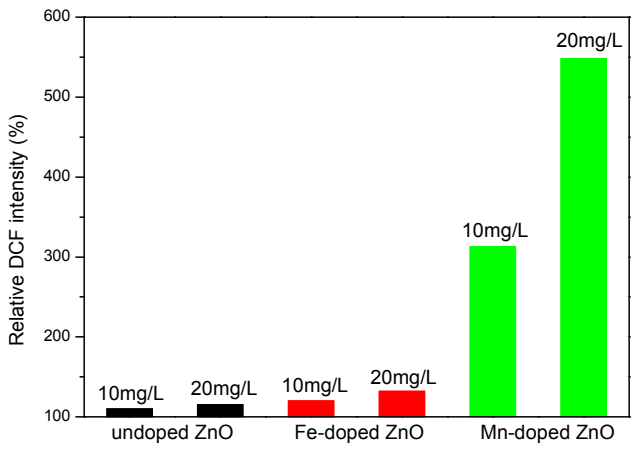

Figure 6 Relative DCF intensities produced by doped or undoped ZnO NPs (compared with the DCF concentration in WIL2-NS cells not exposed to ZnO particles, 100%) when the NP concentration was 10 mg/L and 20 mg/L respectively.

Table 1 Zeta potentials and hydrodynamic sizes measured in deionised water and supplemented RPMI1640 medium

	Zeta potentials in deionised water (mV)	Zeta potentials in supplemented RPMI1640 medium (mV)	Hydrodynamic diameters in deionised water (nm)	Hydrodynamic diameters in supplemented RPMI1640 medium (nm)
Undoped	16.1±0.5	-7.6±0.4	499.1±68.4	868.7±71.6
Fe-doped	12.2±0.4	-9.8±0.9	679.0±171.0	765.2±61.7
Mn-doped	10.6±0.3	-7.6±0.8	516.0±89.2	843.2±103.8